Mechanics of Advanced Materials and Structures (2013) **20**, 122–129

ISSN: 1537-6494 print / 1537-6532 online
DOI: 10.1080/15376494.2011.584140

Effect of Initial Stress on the Lateral Modes in 1-3 Piezocomposites

HONGYAN ZHANG[1,2], YAPENG SHEN[1], YUEMING LI[1], and XUESONG MEI[1]

[1]*School of Aerospace, Xi'an Jiaotong University, Xi'an, P. R. China*
[2]*School of Science, Chang'an University, Xi'an, P. R. China*

Received 21 January 2009; accepted 7 April 2011

An investigation of the effect of initial stress on the lateral modes in 1-3 piezocomposites is conducted. The Governing equations, taking into account the piezoelectricity, initial stress, and initial strain, are developed for the piezocomposites. Analytical solutions of the mechanical displacement and electric potential function are obtained based on the Bloch waves theory. Influence of the initial stress on the lateral modes frequencies and the stop band are discussed in detail, respectively. The conclusion reached indicates that the lateral mode frequencies increase with the piezoelectricity of the piezocomposites, but decrease with the poling initial stress in piezocomposites.

Keywords: 1–3 Piezocomposites, Lateral Modes, Initial Stress, Analytical solutions

1. Introduction

1-3 piezocomposites consist of piezoelectric rods or fibers in a passive polymer matrix. Due to their low acoustic impedance, low mechanical quality and their high electromechanical coupling coefficient, they are well suited for ultrasonic transducers in non destructive testing and medical imaging applications.

While 1-3 piezocomposites offer significant advantages over solid piezoceramic devices, the new microstructure results in the introduction of additional lateral vibration modes, which give rise to spurious resonances [1]. The spurious resonances, caused by the Bragg diffraction of Lamb waves in the periodic microstructure, were first experienced by Gururaja et al. [1]. Gomez et.al. [2] experimentally studied the relevance of the stiffness, impedance, and attenuation coefficient of the polymer in the lateral vibration modes in the 1-3 piezocomposites. The lateral resonances in 3-D periodic layers of finite thickness were explored theoretically by Auld and Wang [3] and Wang [4] using the Floquet formalism. Other authors [5, 6] studied lateral resonances by using the finite element methods. Since these approaches require intensive calculations, a simpler model is highly desired. Certon et al. [7, 8] investigated the propagation of purely transverse waves in a 2-D periodic medium of infinite thickness by using the Bloch waves theory and membrane method. The Bloch waves theory was first developed in the area of solid state physics to calculate the energy bands in a crystal lattice [9]. This approach was described by Wang and Auld [10] in general terms for elastic propagation in 3-D periodic medium and they applied it to the particular case of a 1-D periodic structure. In reference [8], the Bloch waves theory was extended to a 2-D periodic structure. The dispersion curves, the stop band limits, as well as the frequencies and the displacement fields of the lateral modes were obtained and compared with experimental results. However, they did not take into account the piezoelectricity effects. Wilm et al. [11] developed a full 3D model based on a plane wave expansion method for general piezoelectric-based composite materials. Complementary quantitative calculations were performed for thickness modes in 1-3 piezocomposites and compared to a well-established theory.

In most cases, 1-3 piezoelectric composites are prepared from unpoled PZT and the polymer matrix [12, 13]. During the poling process, the PZT tries to elongate in the poling direction and contract in the transverse direction. However, the deformation of the PZT in piezocomposites is hindered by the surrounding polymer, which results in the occurrence of residual stresses in composites. In fact, the residual stresses play a significant role in lateral modes of composites. They will change the lateral mode frequencies and stopbands of piezocomposites. Most previous works gave much attention to the effects of geometry and physical properties on the lateral modes in piezocomposites. Consequently, so far investigations related to the study of the influence of initial stress due to the poling process on the lateral modes in piezocomposites have not been carried out. This article presents an analytical solution based on the use of the Bloch waves theory to study the influence of initial stress on the lateral modes in 1-3 piezoelectric composites. In Section 2, the governing equations with the modified piezoelastic parameters in the stressed

Address correspondence to Hongyan Zhang, School of Aerospace, Xi'an Jiaotong University, Xi'an 710049, P. R. China. E-mail: hong_yan_zhang@126.com

piezocomposites are founded. According to the Bloch waves theory, the analytical solutions for the displacement and electric potential functions are constructed in the reciprocal lattice. A numerical example is given and the effect of the initial stress on the lateral modes is discussed in Section 3, and the concluding remarks are finally made in Section 4.

2. Fundamental Formulations and Solutions

2.1. *Governing Equations in a Prestressed Piezoelectric Medium*

When a continuum medium undergoes deformation, the motion of a material point can be described by [14]:

$$x_k = x_k\,(X_K, t), \quad K = \mathrm{I, II, III}, \quad k = 1, 2, 3, \tag{1}$$

where t denotes time, X denotes a particle position at the natural undeformed configuration, and x denotes its position at current configuration. The subscripts K and k denote the components in the Lagrangian coordinate system at undeformed configuration and the Eulerian coordinate system at current configuration, respectively. The gradient equations are

$$\varepsilon_{KL} = \frac{1}{2}(x_{k,K}x_{k,L} - \delta_{KL}),\; E_K = -\phi_{,K}. \tag{2}$$

The equations of motion [14] without body force and the electric equation without volume charge in the undeformed configuration are

$$(\sigma_{KL}x_{l,L})_{,K} = \rho\ddot{u}_l, \tag{3}$$
$$D_{K,K} = 0. \tag{4}$$

In Eqs. (2)–(5), $\boldsymbol{\sigma}$ stands for the second Piola-Kirchhoff stress tensor, $\boldsymbol{\varepsilon}$ is the Green strain tensor, ρ is the mass density, $\mathbf{D}$ is the electric displacement, $\mathbf{E}$ is the electric field vector, and ϕ is the electric potential. All the above variables are measured at the natural configuration. δ_{KL} is the Kronecker delta, a comma at the subscript position denotes space-coordinate differentiation, and a dot over the letter denotes the time differentiation. The following calculations are carried out within the quasi static hypothesis.

In practical cases, a mechanical biasing state produced by initial poling stresses is in an equilibrium state. Applying the external dynamic mechanical or electrical loads, the body is further perturbed by an additional wave motion of small amplitude onto the initial state. Let

$$\sigma^t_{KL} = \sigma^0_{KL} + \sigma_{KL}, \quad u^t_l = u^0_l + u_l, \quad D^t_K = D^0_K + D_K, \tag{5}$$

where σ^t_{KL} and D^t_K are the total Kirchhoff stress and total electric displacement referred to the natural state and u^t_l is the total displacement at Euler coordinate system. σ_{KL}, D_K, and u_l are their incremental values. The subscript "0" denotes the variables in the initial state. Subtracting the equations of motion in the initial state from those in the perturbed state and neglecting the small higher-order quantities, we can obtain the expected governing wave equation in the natural configuration (for more details, please see reference [15]):

$$\left(\sigma_{KL}\,\delta_{lL} + \sigma^0_{KL}\,u_{l,L} + \sigma_{KL}\,u^0_{l,L}\right)_{,K} + \rho f_l = \rho\ddot{u}_l. \tag{6}$$

In practical calculation, the Eulerian coordinate system is assumed to coincide with the Lagrangian coordinate system. Thus, Eq. (6) can be rewritten as:

$$\left(\sigma_{ij} + \sigma^0_{ik}u_{j,k} + \sigma_{ik}u^0_{j,k}\right)_{,i} + \rho f_j = \rho\ddot{u}_j \qquad i, j, k = 1, 2, 3. \tag{7}$$

The constitutive equations of the piezoelectric ceramic are [14, 15]

$$\sigma^t_{ij} = C_{ijkl}\,\varepsilon^t_{kl} + \frac{1}{2}C_{ijklmn}\,\varepsilon^t_{kl}\,\varepsilon^t_{mn} - e_{mij}\,E^t_m - e_{mijkl}\,\varepsilon^t_{kl}\,E^t_m - \frac{1}{2}l_{mnij}\,E^t_m E^t_n + h.o.t, \tag{8a}$$

$$D^t_m = e_{mij}\,\varepsilon^t_{ij} + \frac{1}{2}e_{mijkl}\,\varepsilon^t_{ij}\,\varepsilon^t_{kl} + \in_{mn}\; E^t_n + \frac{1}{2}\in_{mnp}\,E^t_n E^t_p + l_{mnij}E^t_n\,\varepsilon^t_{ij} + h.o.t, \tag{8b}$$

where $i, j, k, l, m, n, p = 1, 2, 3$, C_{ijkl}, and C_{ijklmn} are the second- and third-order elastic constants at constant electrical displacement, e_{mij} and e_{mijkl} are the second- and third-order piezoelectric constants, $\in_{mn}$ and $\in_{mnp}$ are the second- and third-order dielectric constants at constant strain, and l_{mnij} is the electrostrictive constant. Subtracting the constitutive equations in the initial state from those in the disturbed state and neglecting the higher-order terms, we can get:

$$\sigma_{ij} = \hat{C}_{ijkl}u_{k,l} + \hat{e}_{mij}\phi_{,m}, \tag{9a}$$
$$D_m = e^*_{mij}u_{i,j} - \in^*_{mn}\,\phi_{,n}, \tag{9b}$$

where

$$\begin{aligned}
\hat{C}_{ijkl} &= C_{ijkl} + (C_{ijnl}\delta_{km} + C_{ijklmn})u^0_{m,n} + e_{mijkl}\phi^0_{,m},\\
\hat{e}_{mij} &= e_{mij} + e_{mijkl}u^0_{k,l} - l_{mnij}\phi^0_{,n},\\
e^*_{mij} &= e_{mij} + (e_{mil}\,\delta_{jk} + e_{mijkl})\,u^0_{k,l} - l_{mnij}\,\phi^0_{,n},\\
\in^*_{mn} &= \in_{mn} + l_{mnij}\,u^0_{i,j} - \in_{mnp}\;\phi^0_{,p}.
\end{aligned} \tag{10a–d}$$

If we define $C^*_{ijkl} = \hat{C}_{ijkl} + C_{inkl}\delta_{jm}u^0_{m,n}$, substituting Eq. (9) into Eqs. (4) and (7), we get [16]:

$$\left(\sigma^*_{ij} + u_{j,k}\sigma^0_{ik}\right)_{,i} + \rho f_j = \rho\ddot{u}_j, \tag{11}$$
$$D_{i,i} = 0, \tag{12}$$

where

$$\sigma^*_{ij} = C^*_{ijkl}u_{k,l} + e^*_{mij}\phi_{,m}, \tag{13a}$$
$$D_m = e^*_{mij}u_{i,j} - \in^*_{mn}\,\phi_{,n}, \tag{13b}$$

where C^*_{ijkl}, e^*_{mij}, and $\in^*_{mn}$ are effective elastic, piezoelectric, and dielectric constants, respectively. If $u^0_{i,j}$ is small, then $\sigma^*_{ij} = \sigma_{ij}$.

In the following text for convenience, σ_{ij}^* is replaced by σ_{ij}, but it should be noted that they are different from those σ_{ij} in previous equations.

2.2. *Governing Equations in the Prestressed 1-3 Piezocomposites*

The 2-D geometry of 1-3 piezocomposites is illustrated in Figure 1. The Cartesian x, y, z co-ordinate system is used, with x, y corresponding to the cross section of the composite and z corresponding to the poling direction. d_p is the ceramic rod width, and $d$is the pitch of the structures. Due to the fact that piezoelectric pillars are in square pitch arrangement, we assume 1-3 piezocomposites are transversally isotropic. Following Voigt notation: 11–1, 22–2, 33–3, 23–4, 13–5, 12–6, for a z-polarized wave propagating in the x-y plane at frequency ω, Eq. (13) reduces to:

$$\frac{\partial}{\partial x}\left[\left(C_{44}^*+\sigma_{xx}^{(0)}\right)\frac{\partial w}{\partial x}+\sigma_{xy}^{(0)}\frac{\partial w}{\partial y}+e_{15}^*\frac{\partial \phi}{\partial x}\right] + \frac{\partial}{\partial y}\left[\left(C_{44}^*+\sigma_{yy}^{(0)}\right)\frac{\partial w}{\partial y}+\sigma_{xy}^{(0)}\frac{\partial w}{\partial x}+e_{15}^*\frac{\partial \phi}{\partial y}\right]=-\rho\omega^2 w, \tag{14}$$

$$\frac{\partial}{\partial x}\left(e_{15}^*\frac{\partial w}{\partial x}-\in_{11}^*\frac{\partial \phi}{\partial x}\right)+\frac{\partial}{\partial y}\left(e_{15}^*\frac{\partial w}{\partial y}-\in_{11}^*\frac{\partial \phi}{\partial y}\right)=0, \tag{15}$$

where w is the displacement along direction z.

In the following calculations, all quantities taken in the piezoelectric phase are marked with the letter "p" while the letter "r" distinguishes those in the polymer phase. The mean value of the function $C_{ij}(x, y)$, calculated using the definition of the mean value of a periodic function, is given by:

$$\bar{C}_{ij}^* = \frac{\int_{-d/2}^{+d/2}\int_{-d/2}^{+d/2} C_{ij}^*(x,y)dxdy}{\int_{-d/2}^{+d/2}\int_{-d/2}^{+d/2} dxdy} = \left(\frac{d_p}{d}\right)^2 C_{ij}^{*p} + \left[1-\left(\frac{d_p}{d}\right)^2\right] C_{ij}^{*r}. \tag{16}$$

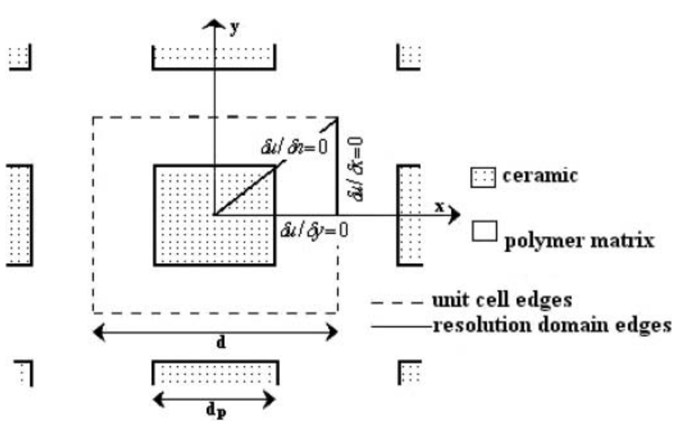

Fig. 1. Geometry of 2-D periodic medium (d_p is the ceramic rod width and d is the pitch).

In a similar way, one gets the mean values of the functions $\rho(x, y)$, $e_{ij}^*(x, y)$, $\in_{ij}^*(x, y)$, and $\sigma_{ij}^{(0)}(x, y)$. Then the material coefficients and initial stress in 1-3 piezocomposites can be expressed as:

$$\begin{aligned} &C_{ij}^*(x,y)=\bar{C}_{ij}^*+\delta C_{ij}(x,y), \quad \rho(x,y)=\bar{\rho}+\delta\rho(x,y),\\ &e_{ij}^*(x,y)=\bar{e}_{ij}^*+\delta e_{ij}(x,y), \quad \in_{ij}^*(x,y)=\bar{\in}_{ij}^*+\delta\in_{ij}(x,y),\\ &\sigma_{ij}^{(0)}(x,y)=\bar{\sigma}_{ij}^{(0)}+\delta\sigma_{ij}^{(0)}(x,y), \end{aligned} \tag{17a–e}$$

where the notaion "δ" represents the spatial variations of the corresponding quantities around their mean value. Substituting Eqs. (17a)–(17e) into Eqs. (14) and (15), one gets:

$$\begin{aligned} &\left(\bar{C}_{44}^*+\bar{\sigma}_{xx}^{(0)}\right)\frac{\partial^2 w}{\partial x^2}+\left(\bar{C}_{44}^*+\bar{\sigma}_{yy}^{(0)}\right)\frac{\partial^2 w}{\partial y^2}+2\bar{\sigma}_{xy}^{(0)}\frac{\partial^2 w}{\partial x\partial y}\\ &\quad+\bar{e}_{15}^*\left(\frac{\partial^2\phi}{\partial x^2}+\frac{\partial^2\phi}{\partial y^2}\right)+\bar{\rho}\omega^2 w\\ &\quad=-\left[\left(\delta C_{44}+\delta\sigma_{xx}^{(0)}\right)\frac{\partial^2 w}{\partial x^2}+\left(\delta C_{44}+\delta\sigma_{yy}^{(0)}\right)\frac{\partial^2 w}{\partial y^2}\right.\\ &\quad\left.+\ 2\delta\sigma_{xy}^{(0)}\frac{\partial^2 w}{\partial x\partial y}+\delta e_{15}\left(\frac{\partial^2\phi}{\partial x^2}+\frac{\partial^2\phi}{\partial y^2}\right)+\delta\rho\omega^2 w\right]\\ &\quad-\left\{\left[\frac{\partial\left(\delta C_{44}+\delta\sigma_{xx}^{(0)}\right)}{\partial x}+\frac{\partial\delta\sigma_{xy}^{(0)}}{\partial y}\right]\frac{\partial w}{\partial x}\right.\\ &\quad+\left[\frac{\partial\left(\delta C_{44}+\delta\sigma_{yy}^{(0)}\right)}{\partial y}+\frac{\partial\delta\sigma_{xy}^{(0)}}{\partial x}\right]\frac{\partial w}{\partial y}+\frac{\partial\delta e_{15}}{\partial x}\frac{\partial\phi}{\partial x}\\ &\quad\left.+\frac{\partial\delta e_{15}}{\partial y}\frac{\partial\phi}{\partial y}]\right\}, \end{aligned} \tag{18}$$

$$\begin{aligned} &\bar{e}_{15}^*\left(\frac{\partial^2 w}{\partial x^2}+\frac{\partial^2 w}{\partial y^2}\right)-\bar{\in}_{11}^*\left(\frac{\partial^2\phi}{\partial x^2}+\frac{\partial^2\phi}{\partial y^2}\right)\\ &\quad=-\left[\delta e_{15}\left(\frac{\partial^2 w}{\partial x^2}+\frac{\partial^2 w}{\partial y^2}\right)-\delta\in_{11}\left(\frac{\partial^2\phi}{\partial x^2}+\frac{\partial^2\phi}{\partial y^2}\right)\right]\\ &\quad-\left[\left(\frac{\partial\delta e_{15}}{\partial x}\frac{\partial w}{\partial x}+\frac{\partial\delta e_{15}}{\partial y}\frac{\partial w}{\partial y}\right)-\left(\frac{\partial\delta\in_{11}}{\partial x}\frac{\partial\phi}{\partial x}+\frac{\partial\delta\in_{11}}{\partial y}\frac{\partial\phi}{\partial y}\right)\right]. \end{aligned} \tag{19}$$

2.3. *Solution*

According to the Bloch waves theory [9], the solutions for the displacement and electric potential in such periodic structures must satisfy the Bloch periodicity condition, which can be expressed as:

$$w(\mathbf{r}+\mathbf{T}_{m,n})=w(\mathbf{r})e^{\mathbf{j}\mathbf{k}_0\cdot\mathbf{T}_{m,n}}, \tag{20}$$
$$\phi(\mathbf{r}+\mathbf{T}_{m,n})=\phi(\mathbf{r})e^{\mathbf{j}\mathbf{k}_0\cdot\mathbf{T}_{m,n}}, \tag{21}$$

where $\mathbf{r}$ is the position vector given by $\mathbf{r}=x\mathbf{i}+y\mathbf{j}$, $\mathbf{k}_0$ is the wave vector of the incident plane wave in the first Brillouin zone of the space, and $\mathbf{T}_{m,n}=md\mathbf{i}+nd\mathbf{j}$ (m and n are integers) are the lattice translation vectors. In order to satisfy Eqs. (20) and (21), the solutions for the displacement w and electric potential ϕ must be expressed as Bloch functions [9],

$$w(x, y, t) = F(\mathbf{r})e^{j(\omega t - \mathbf{k}_0 \cdot \mathbf{r})}, \tag{22}$$
$$\phi(x, y, t) = G(\mathbf{r})e^{j(\omega t - \mathbf{k}_0 \cdot \mathbf{r})}. \tag{23}$$

Note that displacement w and electric potential ϕ are functions of both space and time. $F(\mathbf{r})$ and $G(\mathbf{r})$ are scalar periodic functions of the space with period d. Therefore, they can be expanded as double Fourier series in the reciprocal lattice,

$$F(\mathbf{r}) = \sum_{m,n=-\infty}^{m,n=+\infty} a_{mn} e^{-j(\mathbf{K}_{mn} \cdot \mathbf{r})}, \tag{24}$$
$$G(\mathbf{r}) = \sum_{m,n=-\infty}^{m,n=+\infty} b_{mn} e^{-j(\mathbf{K}_{mn} \cdot \mathbf{r})}, \tag{25}$$

where $\mathrm{K}_{mn} = (2\pi/d)m\,\mathrm{i} + (2\pi/d)n\,\mathrm{j}$ are the reciprocal lattice vectors. By substituting Eqs. (24) and (25) into Eqs. (22) and (23), the solutions of the present problem are represented as:

$$w(x, y, t) = \left[\sum_{m,n=-\infty}^{m,n=+\infty} a_{mn} e^{-j(\mathbf{k}_{mn} \cdot \mathbf{r})}\right] e^{j\omega t}, \tag{26}$$
$$\phi(x, y, t) = \left[\sum_{m,n=-\infty}^{m,n=+\infty} b_{mn} e^{-j(\mathbf{k}_{mn} \cdot \mathbf{r})}\right] e^{j\omega t}, \tag{27}$$

with $\mathbf{k}_{mn} = \mathbf{K}_{mn} + \mathbf{k}_0$.

For a given wave vector $\mathbf{k_0}$, the solutions $w(x, y)$ and $\phi(x, y)$ can be obtained by calculating the coefficients a_{mn} and b_{mn}. Inserting Eqs. (26) and (27)into the coupled governing Eqs. (18) and (19), and then using the orthogonality property of Fourier series components yield the following expressions for the propagation equation and the Poisson's condition:

$$\begin{aligned}
&\big[\bar{\rho}\omega^2 - \bar{C}^*_{44}\,|\mathbf{k}_{mn}|^2 - \big(\bar{\sigma}^{(0)}_{xx} k^2_{mn(x)} + \bar{\sigma}^{(0)}_{yy} k^2_{mn(y)}\big) \\
&\quad - 2\bar{\sigma}^{(0)}_{xy} k_{mn(x)} k_{mn(y)}\big] a_{mn} + \big(-\bar{e}^*_{15}\,|\mathbf{k}_{mn}|^2\big) b_{mn} \\
&\quad = -\left(\sum_{p,q} K_{mnpq} a_{pq} + \sum_{p,q} L_{mnpq} b_{pq}\right),
\end{aligned} \tag{28}$$

$$\begin{aligned}
&\big(-\bar{e}^*_{15}\,|\mathbf{k}_{mn}|^2\big) a_{mn} + \big(\bar{\epsilon}^*_{11}\,|\mathbf{k}_{mn}|^2\big) b_{mn} \\
&\quad = -\left(\sum_{p,q} L_{mnpq} a_{pq} + \sum_{p,q} N_{mnpq} b_{pq}\right),
\end{aligned} \tag{29}$$

$$m, n \to -\infty \text{ to } +\infty,\ \ p, q \to -\infty \text{ to } +\infty,$$

where $\mathbf{K}_{mn} = K_{mn(x)}\,\mathbf{i} + K_{mn(y)}\,\mathbf{j}$ and $\mathbf{k}_{pq} = k_{pq(x)}\,\mathbf{i} + k_{pq(y)}\,\mathbf{j}$. Here, if $m \neq p$ or $n \neq q$,

$$\begin{aligned}
K_{mnpq} &= \big[\Delta\rho\,\omega^2 - \Delta C^*_{44}\mathbf{k}_{mn} \cdot \mathbf{k}_{pq} \\
&\quad - \big(\Delta\sigma^{(0)}_{xx} k_{mn(x)} k_{pq(x)} + \Delta\sigma^{(0)}_{yy} k_{mn(y)} k_{pq(y)}\big) \\
&\quad - \big(k_{mn(x)} k_{pq(y)} + k_{mn(y)} k_{pq(x)}\big)\Delta\sigma^{(0)}_{xy}\big]\frac{d_p^2}{d^2} \\
&\quad \times \sin c\left(\frac{\pi(m-p)d_p}{d}\right) \sin c\left(\frac{\pi(n-q)d_p}{d}\right),
\end{aligned} \tag{30a}$$

$$\begin{aligned}
L_{mnpq} &= \big(-\Delta e^*_{15}\mathbf{k}_{mn} \cdot \mathbf{k}_{pq}\big)\frac{d_p^2}{d^2} \\
&\quad \times \sin c\left(\frac{\pi(m-p)d_p}{d}\right) \sin c\left(\frac{\pi(n-q)d_p}{d}\right),
\end{aligned} \tag{30b}$$

$$\begin{aligned}
N_{mnpq} &= \big(\Delta \epsilon^*_{11}\,\mathbf{k}_{mn} \cdot \mathbf{k}_{pq}\big)\frac{d_p^2}{d^2} \\
&\quad \times \sin c\left(\frac{\pi(m-p)d_p}{d}\right) \sin c\left(\frac{\pi(n-q)d_p}{d}\right),
\end{aligned} \tag{30c}$$

if $m = p$ and $n = q$,

$$K_{mnpq} = L_{mnpq} = N_{mnpq} = 0, \tag{31}$$

with

$$\Delta C^*_{44} = C^{*p}_{44} - C^{*r}_{44}, \quad \Delta\rho = \rho^p - \rho^r, \quad \Delta e^*_{15} = e^{*p}_{15} - e^{*r}_{15},$$
$$\Delta \epsilon^*_{11} = \epsilon^{*p}_{11} - \epsilon^{*r}_{11}, \quad \Delta\sigma^{(0)}_{ij} = \sigma^{(0)p}_{ij} - \sigma^{(0)r}_{ij}. \tag{32a–e}$$

Further details concerning the calculation of the coefficients K_{mnpq} are given in Appendix A. In order to simplify the calculation of the lateral mode frequencies and the solutions of displacement and electric potential, we rearrange Eqs. (28) and (29) as:

$$\sum_{p,q} \hat{K}_{mnpq} a_{pq} + \sum_{p,q} \hat{L}_{mnpq} b_{pq} = 0, \tag{33}$$
$$\sum_{p,q} \hat{L}_{mnpq} a_{pq} + \sum_{p,q} \hat{N}_{mnpq} b_{pq} = 0. \tag{34}$$

If $m \neq p$ or $n \neq q$:

$$\hat{K}_{mnpq} = K_{mnpq}; \quad \hat{L}_{mnpq} = L_{mnpq}; \quad \hat{N}_{mnpq} = N_{mnpq}; \tag{35a–c}$$

if $m = p$ and $n = q$:

$$\begin{aligned}
\bar{K}_{mnpq} &= \omega^2\bar{\rho} - \big[\big(\bar{\sigma}^{(0)}_{xx} + \bar{C}^*_{44}\big)k^2_{mn(x)} + \big(\bar{\sigma}^{(0)}_{yy} + \bar{C}^*_{44}\big)k^2_{mn(y)} \\
&\quad + 2\bar{\sigma}^{(0)}_{xy} k_{mn(x)} k_{mn(y)}\big], \\
\bar{L}_{mnpq} &= -\bar{e}^*_{15}\,|\mathbf{k}_{mn}|^2, \\
\bar{N}_{mnpq} &= \bar{\epsilon}^*_{11}\,|\mathbf{k}_{mn}|^2.
\end{aligned} \tag{36a–c}$$

In numerical calculations, one can assume $N \times N$ terms in the Fourier expansions of Eqs. (24) and (25). For non-trivial solutions, the determinant of coefficients of Eqs. (33) and (34) should vanish, which gives the frequency ω. Furthermore, the coefficients a_{mn} and b_{mn} can be obtained from the eigenvectors, and the dispersion curves can also be calculated by fixing the wave vector $\mathbf{k}_0$.

3. Numerical Results and Discussion

In order to illustrate the effect of the poling initial stress on the lateral modes in piezocomposites, a 1-3 piezoelectric composite was considered. As shown in Figure 1, the ceramic rod

Table 1. Material parameters

Materials	Elastic constant, $C_{44}(10^{10}\ \mathrm{N/m^2})$	Mass density, $\rho(10^3\ \mathrm{kg/m^3})$	Piezoelectric constant, $e_{15}(\mathrm{c/m^2})$	Dielectric constant, $\in_{11}(10^{-10}\ \mathrm{F/m})$
PZT ceramic	4.2	7.50	17.0	150.45
Polymer matrix	0.17	1.15	0.0	0.398

width is 50 μm and the width-to-pitch ratio is 0.5. The second-order material constants used in the analysis were listed in Table 1. For the third-order material constants, please see Appendix B.

3.1. *Dispersion Curves and Stop Bands*

Gururaja et al. [1] has shown that two directions of propagation for the calculation of the first two lateral modes are in the direction of the vectors **i** and (**i** + **j**). Therefore, the solutions are, respectively, calculated between $|\mathbf{k_0}| = 0$ and $|\mathbf{k_0}| = \pi/d$ along the directions of the vector **i** and (**i** + **j**).

For $k_0 d/\pi$ or $k_0 d/\pi\sqrt{2}$ equal to 0 or 1, the incident wave vector $\mathbf{k_0}$ is at the edge of a Brillouin zone where the Bragg diffraction condition is satisfied and corresponds to resonant standing waves. First, the lateral mode frequencies in two cases that include and do not include the coupling coefficients are calculated at $|\mathbf{k_0}| = 0$, and the results are listed in Table 2. It is clear that the present formulation predicts exactly the same frequencies as that shown in reference [8] by setting the coupling material coefficients e_{15}^p, $\in_{11}^p$, and $\in_{11}^r$ to be zero. Furthermore, the lateral modes frequencies in case 2 are higher than that in case 1. The differences in lateral mode frequencies between two cases are a consequence of the stiffening effect that the piezoelectric terms generate. In general, these terms tend to increase the overall stiffness of the piezocomposites because of the internal forces generated by the induced electric field.

Second, dispersion relations of propagation modes in 1-3 piezocomposites with poling initial stress are demonstrated in Figures 2 and 3. These dispersion relations depict a full spectrum of dynamic behavior of the composites. In the calculation, the initial stress in each phase of the 1-3 piezocomposites along direction x equals that along direction y for the transverse-isotropy of the composites. We assume that the initial stress is independent of x and y throughout the individual phase. This is clearly not true in detail, as finite-element calculations reveal. The expectation is that this approximation captures the physical behavior in an average sense. According to references [16] and [17], the values of initial stresses and

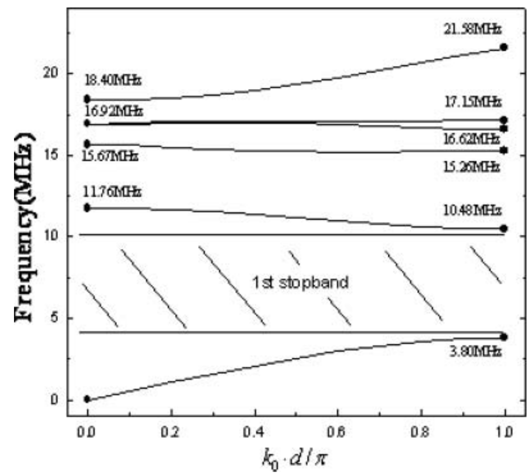

Fig. 2. Dispersion curve of shear wave propagating along the x axis.

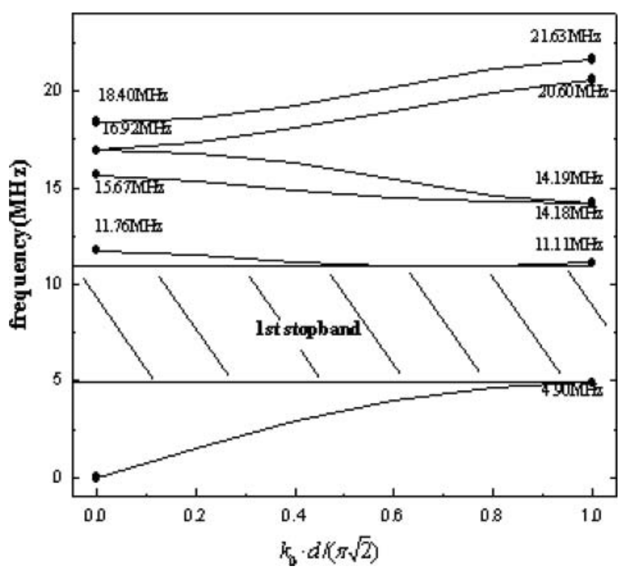

Fig. 3. Dispersion curve of shear wave propagating along the line x = y.

Table 2. The lateral mode frequencies in 1–3 piezocomposites for different cases

Different cases	Coupling coefficients	Frequencies (MHz) $[\lvert\mathbf{k_0}\rvert = 0]$					
Paper [10]	—	0	11.57	15.45	16.53	16.53	18.23
Case 1	$\sigma_{ij}^{(0)} = 0$; $e_{15}^p = 0$; $\in_{11}^p = 0$	0	11.57	15.45	16.53	16.53	18.23
Case 2	$\sigma_{ij}^{(0)} = 0$; $e_{15}^p \neq 0$; $\in_{11}^p \neq 0$	0	11.77	15.67	16.94	16.94	18.40

Table 3. The lateral mode frequencies in 1–3 piezocomposites with different initial stress cases

$\sigma_{xy}^{(0)p}$ MPa	$\sigma_{xy}^{(0)r}$ MPa	$\sigma_{xx}^{(0)p} = \sigma_{yy}^{(0)p}$ MPa	$\sigma_{xx}^{(0)r} = \sigma_{yy}^{(0)r}$ MPa	Frequencies (MHz)					
0	0	0	0	0.0	11.7635	15.6690	16.9270	16.9282	18.3978
		1.11	0	0.0	11.7636	15.6691	16.9271	16.9283	18.3979
		0	−0.37	0.0	11.7622	15.6674	16.9253	16.9265	18.395
		1.11	−0.37	0.0	11.7623	15.6675	16.9254	16.9266	18.3960
0.58	0.29	1.11	−0.37	0.0	11.7623	15.6675	16.9259	16.9260	18.3959

initial strains are determined, that is,

$$\begin{aligned}
\sigma_{xx}^{(0)p} &= \sigma_{yy}^{(0)p} = 1.11\text{MPa}, \quad \sigma_{xy}^{(0)p} = 0.58\text{MPa} \\
\sigma_{xx}^{(0)r} &= \sigma_{yy}^{(0)r} = -0.37\text{MPa}, \quad \sigma_{xy}^{(0)r} = 0.29\text{MPa}, \\
\varepsilon_{xx}^{(0)p} &= \varepsilon_{yy}^{(0)p} = -9.54 \times 10^{-4}, \quad \varepsilon_{zz}^{(0)p} = 1.88 \times 10^{-3}, \\
\varepsilon_{xx}^{(0)r} &= \varepsilon_{yy}^{(0)r} = -3.86 \times 10^{-4}, \quad \varepsilon_{zz}^{(0)r} = 1.02 \times 10^{-4}.
\end{aligned}$$

It is obvious that the width of the stop band for the case that includes the piezoelectricity and initial stress is broader than that of the case where piezoelectricity and initial stress are not taken into account (refer to reference [8]).

For resonances where $k_0 d/\pi$ or $k_0 d/\pi\sqrt{2}$ equals 1, the adjacent ceramic rods are separated by an odd number of half-wavelengths, so their vibrations are 180° out of phase. These resonances are not electrically coupled [8]. On the other hand, when $k_0 d/\pi$ or $k_0 d/\pi\sqrt{2}$ is equal to 0, all the ceramic rods vibrate in phase. Furthermore, these displacement fields are either symmetrical or antisymmetrical, due to the transduction effect, only the former are piezoelectrically coupled. Since the symmetrical displacement fields are demanded, from Figures 2 and 3, 11.76 and 18.40 MHz are the first and second lateral modes.

3.2. *Effect of Initial Stress on the Lateral Mode Frequencies*

In order to investigate the influence of initial stress in each phase on the lateral mode frequencies, five different initial stress cases are considered as follows:

1. without the initial stress;
2. only initial normal stress in the ceramic is considered;
3. only initial normal stress in the matrix is considered;
4. only initial normal stresses in the composites are considered; and
5. the real initial stress condition (including initial normal stress and initial shear stress in the composites).

With $|\mathbf{k_0}| = 0$, the lateral mode frequencies in the above five cases are calculated and listed in Table 3. The analysis of these results shows that the compressive initial stress in the matrix tends to decrease the lateral mode frequencies, but the tensile initial stress in the ceramic tends to increase the frequencies. Furthermore, the influence of initial compressive stress in the matrix is more significant than that of initial tensile stress in the ceramic. Compared with the influence of initial normal stress, the influence of shear stress on the lateral modes is tiny. Thus, in the real initial stress condition, the poling initial stress would decrease the lateral mode frequencies. By comparing the numerical results shown in Tables 2 and 3, we can find that the influence of piezoelectricity on the lateral modes is more obvious than that of the initial stress.

Figures 4 and 5 show the plots of the first and second lateral mode frequencies versus the initial normal stress in the matrix, respectively. Here, only the initial normal stress in the matrix is changed while keeping other initial stresses fixed. The numerical results also demonstrate that the lateral mode frequencies almost decrease linearly with the increase of the magnitude of the initial normal stress in the matrix.

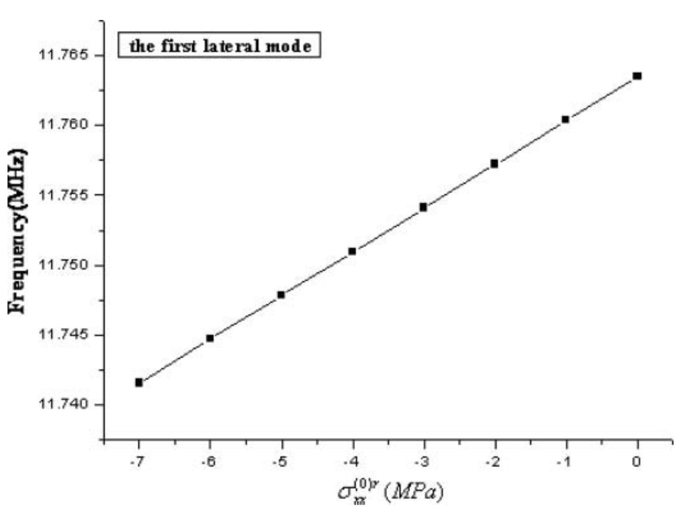

Fig. 4. The first lateral mode versus different initial stress in the matrix.

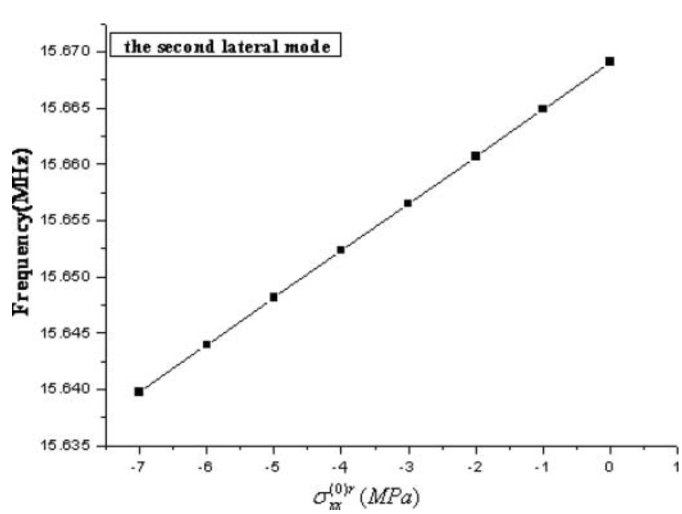

Fig. 5. The second lateral mode versus different initial stress in the matrix.

4. Conclusions

The lateral modes in 1-3 piezocomposites with initial stress have been investigated using an analytical method. The initial stresses and initial strains terms have been included in the governing equations. The wave equations have been solved based on the Bloch waves theory. Results show that the effects of the initial stress and piezoelectricity of composites on the lateral modes are significant.

The lateral mode frequencies rise and the stop band broadens due to the effects of piezoelectric characteristics of composites. The lateral mode frequencies increase with the initial tensile stress in the ceramic phase and decrease with the initial compressive stress in the matrix. The influence of the initial compressive stress in the matrix on the lateral mode frequencies is more significant than that of the initial tensile stress in the ceramic. Furthermore, compared with that of the initial normal stress, the influence of the initial shear stress is tiny. Thus, the poling initial stress tends to decrease the lateral mode frequencies in the real initial stress condition.

Acknowledgments

The authors would like to acknowledge the support of the China Postdoctoral Science Foundation (20090451382), National Natural Science Foundation of China (11002106), and Nature Science Foundation of Shannxi Province (2009JQ1008). This work was also partially supported by the National High Technology Research and Development Program (973 Program, No. 2009CB724402).

References

[1] T.R. Gururaja, W.A. Schulze, L.E. Cross, R.E. Newham, B.A. Auld, and Y.J. Wang, Piezoelectric composites materials for ultrasonic transducer applications. Part I: Resonant modes of vibration of PZT rod-polymer composites, IEEE Trans. Ultrason. Ferroelec. Freq. Contr., vol. SU-32, pp. 481–498, 1985.
[2] H. Gomez, C. Negreira, A. Aulet, J.A. Eiras, and L.A. Bassora, Influence of elastic characteristics of the polymer/resin in later resonances of piezocomposites (1-3), Ultrasonics Symposium 1996: Proceedings, 1996 IEEE, San Antonio, TX, 3–6 November 1996.
[3] B.A. Auld and Y. Wang, Acoustic wave vibrations in periodic composite plates, Ultrasonics Symposium 1984: Proceedings, 1984 IEEE, San Francisco, CA, 14–16 November 1984.
[4] Y. Wang, Waves and vibrations in elastic superlattice composites, Ph.D. Thesis, Stanford University, Stanford, CA, 1986.
[5] J.A. Hossack and G. Hayward, Finite element analysis of composite piezoelectric transducers, IEEE. Trans. Ultrason. Ferroelec. Freq. Contr., vol. 38, pp. 618–629, 1991.
[6] R. Steinhausen, C. Pientschke, W. Seifert, and H. Beige, Finite element analysis of the thickness mode resonance of piezoelectric 1-3 fibre composites, IEEE Ultrasonics Symposium 2004: A Conference of the IEEE International Ultrasonics, Ferroelectrics and Frequency Control Society, Montreal, Quebec, Canada, 23–27 August 2004.
[7] D. Certon, F. Patat, O. Casula, F. Patat, and D. Royer, Theoretical and experimental investigations of lateral modes in 1-3 piezocomposites, IEEE Trans. Ultrason. Ferroelec. Freq. Contr., vol. 44, no. 3, pp. 643–651, 1997.
[8] D. Certon, F. Patat, F. Levassort, G. Feuillard, and B. Karisson, Lateral resonances in 1-3 piezoelectric periodic composite: Modeling and experimental results, J. Acoust. Soc. Am., vol. 101, no. 4, pp. 2043–2051, 1997.
[9] C. Kittel, Introduction to Solid State Physics (5th Ed.), Wiley, New York, Chapter 2, 1976.
[10] Y. Wang and B.A. Auld, Numerical analysis of Bloch theory for acoustic wave propagation in one dimensional periodic composites, ISAF 1986: Proceedings of the Sixth IEEE International Symposium on Applications of Ferroelectrics, Bethlehem, PA, USA, 8–11 June 1986.
[11] M. Wilm, S. Ballandras, V. Laude, and T. Pastureaud, A plane-wave-expansion approach for modeling acoustic propagation in 2D and 3D piezoelectric periodic structures, Ultrasonics Symposium 2001: Proceedings, IEEE, Atlanta, GA, 1–3 May 2001.
[12] S.S. Livneh, V.F. Janas, and Safari Ah, Development of fine scale PZT ceramic fiber/polymer shell composite transducers, J. Am. Ceram. Soc., vol. 78, no. 7, pp. 1900–1906, 1995.
[13] W. Watzka, S. Seifert, H. Scholz, D. Spore, A. Schoenecker, and L. Seffner, Dielectric and ferroelectric properties of 1-3 composites containing thin PZT-fibers, IEEE Int. Symp. Appl. Ferroelec., vol. 2, pp. 569–572, 1996.
[14] Z.B. Kuang, Nonlinear Continuum Mechanics, Shanghai Jiaotong University Press, Shanghai, Chapter 2, 2002.
[15] H. Liu, Z.B. Kuang, and Z.M. Cai, Propagation of Bleustein-Gulyaev waves in a prestressed layered piezoelectric structure, Ultrasonics, vol. 41, pp. 397–405, 2003.
[16] T. Hauke, R. Steinhausen, W. Seifert, and H. Beige, Modeling of poling behavior of ferroelectric 1-3 composites, J. Appl. Phys., vol. 89, no. 9, pp. 5040–5047, 2001.
[17] H.Y. Zhang, L.X. Li, and Y.P. Shen, Modeling of poling behavior of ferroelectric 3-3 composites, Int. J. Eng. Sci., vol. 43, pp. 1138–1156, 2005.

Appendix A: Theoretical Derivation of the Coefficient

The details of the calculation of the coefficients K_{mnpq} are given below;

$$\begin{aligned}&\int_{-d/2}^{+d/2}\int_{-d/2}^{+d/2} e^{j(\mathbf{k}_{mn}-\mathbf{k}_{pq})\cdot\mathbf{r}}dxdy\\&=\int_{-d/2}^{+d/2}\left[\int_{-d/2}^{+d/2} e^{j\frac{2\pi(m-p)}{d}x}dx\right]e^{j\frac{2\pi(n-q)}{d}y}dy\\&=-\frac{1}{\frac{2\pi(m-p)}{d}}\cdot\frac{1}{\frac{2\pi(n-q)}{d}}\left[e^{j\frac{2\pi(m-p)}{d}x}\right]_{-d/2}^{+d/2}\left[e^{j\frac{2\pi(n-q)}{d}y}\right]_{-d/2}^{+d/2}=0,\end{aligned}\tag{A1}$$

$$\begin{aligned}&\int_{-d_p/2}^{+d_p/2}\int_{-d_p/2}^{+d_p/2} e^{j(\mathbf{k}_{mn}-\mathbf{k}_{pq})\cdot\mathbf{r}}dxdy\\&=-\frac{2j\sin\frac{\pi(m-p)d_p}{d}}{\frac{2\pi(m-p)}{d}}\cdot\frac{2j\sin\frac{\pi(n-q)d_p}{d}}{\frac{2\pi(n-q)}{d}}\\&=d_p^2\sin c\left(\frac{\pi(m-p)d_p}{d}\right)\sin c\left(\frac{\pi(n-q)d_p}{d}\right),\end{aligned}\tag{A2}$$

$$\begin{aligned}&\int_{-d/2}^{+d/2}\int_{-d/2}^{+d/2}[\delta\rho\,\omega^2]e^{j(\mathbf{k}_{mn}-\mathbf{k}_{pq})\cdot\mathbf{r}}dxdy\\&=\int_{-d/2}^{+d/2}\int_{-d/2}^{+d/2}\left[-\left(\frac{d_p}{d}\right)^2\Delta\rho\,\omega^2\right]e^{j(\mathbf{k}_{mn}-\mathbf{k}_{pq})\cdot\mathbf{r}}dxdy\end{aligned}$$

$$+\int_{-d_p/2}^{+d_p/2}\int_{-d_p/2}^{+d_p/2}[\Delta\rho\,\omega^2]e^{j(\mathbf{k}_{mn}-\mathbf{k}_{pq})\cdot\mathbf{r}}dxdy$$
$$=\Delta\rho\,\omega^2 d_p^2 \sin c\left(\frac{\pi(m-p)d_p}{d}\right)\sin c\left(\frac{\pi(n-q)d_p}{d}\right), \tag{A3}$$

$$\begin{aligned}
&\int_{-d/2}^{+d/2}\int_{-d/2}^{+d/2}-j\left[k_{pq(x)}\frac{\partial(\delta C_{44}+\delta\sigma_{xx}^{(0)})}{\partial x}\right]e^{j(\mathbf{k}_{mn}-\mathbf{k}_{pq})\cdot\mathbf{r}}dxdy\\
&=\int_{-d/2}^{+d/2}\left[-jk_{pq(x)}\int_{-d/2}^{+d/2}e^{j(\mathbf{k}_{mn}-\mathbf{k}_{pq})\cdot\mathbf{r}}d\big(\delta C_{44}+\delta\sigma_{xx}^{(0)}\big)dy\right.\\
&=\int_{-d/2}^{+d/2}\big[-jk_{pq(x)}(\delta C_{44}+\delta\sigma_{xx}^{(0)})e^{j(\mathbf{k}_{mn}-\mathbf{k}_{pq})\cdot\mathbf{r}}\big]_{-d/2}^{+d/2}dy\\
&\quad+\int_{-d/2}^{+d/2}jk_{pq(x)}\int_{-d/2}^{d/2}(\delta C_{44}+\delta\sigma_{xx}^{(0)})de^{j(\mathbf{k}_{mn}-\mathbf{k}_{pq})\cdot\mathbf{r}}dy\\
&=\int_{-d/2}^{+d/2}\int_{-d/2}^{d/2}-k_{pq(x)}(k_{mn(x)}-k_{pq(x)})\big(\delta C_{44}+\delta\sigma_{xx}^{(0)}\big)\\
&\quad\times e^{j(\mathbf{k}_{mn}-\mathbf{k}_{pq})\cdot\mathbf{r}}dxdy,
\end{aligned}\tag{A4}$$

$$\begin{aligned}
&\int_{-d/2}^{+d/2}\int_{-d/2}^{+d/2}-j\left[k_{pq(y)}\frac{\partial(\delta C_{44}+\delta\sigma_{yy}^{(0)})}{\partial y}\right]e^{j(\mathbf{k}_{mn}-\mathbf{k}_{pq})\cdot\mathbf{r}}dxdy\\
&=\int_{-d/2}^{+d/2}\int_{-d/2}^{d/2}-k_{pq(y)}(k_{mn(y)}-k_{pq(y)})(\delta C_{44}+\delta\sigma_{yy}^{(0)})\\
&\quad\times e^{j(\mathbf{k}_{mn}-\mathbf{k}_{pq})\cdot\mathbf{r}}dxdy.
\end{aligned}\tag{A5}$$

Substituting Eqs. (A1)–(A5) into Eq. (28), we can get:

$$\begin{aligned}
K_{mnpq}&=\big[\Delta\rho\,\omega^2-\Delta C_{44}\mathbf{k}_{mn}\cdot\mathbf{k}_{pq}\\
&\quad-\big(\Delta\sigma_{xx}^{(0)}k_{mn(x)}k_{pq(x)}+\Delta\sigma_{yy}^{(0)}k_{mn(y)}k_{pq(y)}\big)\\
&\quad-\big(k_{mn(x)}k_{pq(y)}+k_{mn(y)}k_{pq(x)}\big)\Delta\sigma_{xy}^{(0)}\big]\frac{d_p^2}{d^2}\\
&\quad\times\sin c\left(\frac{\pi(m-p)d_p}{d}\right)\sin c\left(\frac{\pi(n-q)d_p}{d}\right)
\end{aligned}\tag{A6}$$

Appendix B: Material Constants

Third-order elastic constants of the piezoelectric ceramic in units of 10^{11} N/m^2 (abbreviated notation):

$C_{111}=-21.2$, $C_{112}=-5.3$, $C_{113}=-5.7$, $C_{114}=2.0$,
$C_{123}=-2.5$, $C_{124}=0.4$, $C_{133}=-7.8$, $C_{134}=1.5$,
$C_{144}=-3.0$, $C_{155}=-6.7$, $C_{222}=-23.3$,
$C_{333}=-29.6$, $C_{344}=-6.8$, $C_{444}=-3.0$.

Third-order piezoelectric constants of the piezoelectric ceramic in units of C/m^2:

$e_{115}=17.1$, $e_{116}=-4.7$, $e_{125}=19.9$, $e_{126}=15.9$,
$e_{135}=19.6$, $e_{136}=-0.9$, $e_{145}=20.3$, $e_{311}=14.7$,
$e_{312}=13.0$, $e_{313}=-10.0$, $e_{314}=11.0$, $e_{333}=-17.3$,
$e_{344}=-10.2$.

Third-order elastic constants of polymer in units of 10^{11} N/m^2:

$C_{111}=-2.1$, $C_{112}=-3.45$, $C_{113}=0.12$,
$C_{114}=-1.63$, $C_{123}=-2.94$, $C_{124}=-0.15$,
$C_{133}=-3.12$, $C_{134}=0.02$, $C_{144}=-1.34$,
$C_{155}=-2.0$, $C_{222}=-3.32$, $C_{333}=-8.15$,
$C_{344}=-1.10$, $C_{444}=-2.76$.